

**RESERVE THIS SPACE**

## **Chromic Transitions and Nanomechanical Properties of (Poly)diacetylene Molecular Films**

**Robert W. Carpick<sup>1</sup>, Alan R. Burns<sup>2</sup>, Darryl Y. Sasaki<sup>2</sup>, M. A. Eriksson<sup>3</sup>, Matthew S. Marcus<sup>3</sup>**

<sup>1</sup> **Engineering Physics Dept., University of Wisconsin - Madison, Madison, WI 53704**

<sup>2</sup> **Biomolecular Materials and Interfaces Dept., Sandia National Laboratories, Albuquerque, NM 87185**

<sup>3</sup> **Physics Dept., University of Wisconsin - Madison, Madison, WI 53704**

Polymerization of ultrathin films containing the diacetylene group has produced a variety of robust, highly oriented, and environmentally responsive films with unique chromatic properties. We present recent developments in the preparation and analysis of ultrathin poly(diacetylene) layers on solid substrates, one to three molecular layers thick. This chapter reviews the structural properties, mechanochromism, and in-plane mechanical anisotropy of these films. Atomic force microscopy (AFM) and fluorescence microscopy confirm that the films are organized into highly ordered domains, with the conjugated backbones parallel to the surface. The number of stable layers is affected by the head group functionality. Local mechanical stress applied by AFM and near-field optical probes induces a transition in the film at the nanometer scale involving substantial optical and structural changes. In addition, we show that AFM reveals the relation between the highly anisotropic character of the chromatic polymer backbone and the associated mechanical properties. In particular, we observe that friction depends dramatically upon

**RESERVE THIS SPACE**

the angle between the polymer backbone and the sliding direction, with the maximum found when sliding perpendicular to the backbones. The observed threefold friction and associated structural anisotropy also leads to contrast in the phase response of intermittent-contact AFM, indicating for the first time that in-plane anisotropy of polymeric systems in general can be investigated using this technique.

## Introduction

Ultrathin organic films, prepared through methods such as Langmuir deposition or self-assembly (1,2), offer the possibility of tailoring the optical, mechanical, and chemical properties of surfaces at the molecular scale. Such control of surface properties is required to implement micro- and nano-scale sensors, actuators, and computational devices. Materials that change in response to external stimuli are especially important for such applications. Poly(diacetylene)s (PDAs) (3) merit particular interest as these molecules exhibit strong optical absorption and fluorescence emission that change dramatically with various stimuli, namely optical exposure (*photochromism*) (4-7), heat (*thermochromism*) (8-12), applied stress (*mechanochromism*) (7,13-15), changes in chemical environment (16,17), and binding of specific chemical or biological targets to functionalized PDA side chains (*affinochromism/biochromism*) (18-20). These transitions, along with other properties such as high third-order nonlinear susceptibility, interesting photo-conduction characteristics, and strong nanometer-scale friction anisotropy(21), render PDA a uniquely interesting material.

Optical absorption in PDAs occurs via a  $\pi$ -to- $\pi^*$  absorption within the linear  $\pi$ -conjugated polymer backbone (3). Frequently the first chromic state of the PDA appears blue in color. The chromic transitions described above all involve a significant shift in absorption from low to high energy bands of the visible spectrum, so the PDA transforms from a blue to a red color. The mechanism behind these transitions is not fully established. It is believed that conformational changes such as side chain packing, ordering, and orientation, impart stresses to the polymer backbone that alter its conformation, thus changing the electronic states and the corresponding optical absorption (3,9).

In this chapter, we discuss the Langmuir deposition of ultrathin PDA films and the subsequent measurement of their structural, optical, and mechanical properties at the nanometer scale. By altering the head group functionality, we can choose between mono- and tri-layer PDA film structures. We then show that

we can use the tip of an atomic force microscope (AFM) or a near field scanning optical microscope (NSOM) tip to locally convert the PDA from the blue form to the red form via applied stress. This represents the first time that mechanochromism has been observed at the nanometer scale. Dramatic structural changes are associated with this mechanochromic transition.

AFM measurements also reveal strongly anisotropic friction properties that are correlated with the orientation of the conjugated polymer backbone. The threefold contrast in friction and the associated mechanical anisotropy produces unexpected contrast in intermittent-contact atomic force microscopy (IC-AFM). In IC-AFM, the cantilever tilt breaks the tip-sample rotational symmetry and enables measurements of in-plane anisotropic forces. The anisotropic forces result in varying energy dissipation depending on the cantilever-sample orientation, yielding phase contrast. The unique anisotropic properties of PDA have therefore allowed us to demonstrate very generally that in-plane properties, as opposed to the commonly discussed out-of-plane properties, can be measured with IC-AFM.

## Experimental

### Film Preparation

Details of our materials and sample preparation are described elsewhere (22). Briefly, diacetylene molecules with two distinct head groups were made into separate films (Fig. 1). The first, 10,12-pentacosadiynoic acid (PCDA) (**I**) (Farchan/GFS Chemicals) was received as a bluish powder which was purified to remove polymer content. The second molecule, N-(2-ethanol)-10,12-pentacosadiynamide (PCEA) (**II**) was prepared by coupling ethanolamine with 10,12-pentacosadiynoyl chloride in tetrahydrofuran and triethylamine. The acid chloride was prepared from the PCDA using oxalyl chloride in methylene chloride. PCEA was isolated by flash column chromatography on silica gel (25% ethylacetate/hexanes,  $R_f = 0.23$ ).

Langmuir film preparations were performed on a Langmuir trough (Nima) which was situated on a vibration isolation table inside a class 100 clean room. The pure water subphase was kept at  $15 \pm 0.2$  °C. Diacetylene monomers were spread on the water surface in a 50% chloroform/benzene solution. All films were incubated for 10 – 15 minutes at zero pressure prior to compression.

For polymerization at the air-water interface, the films were compressed to a surface pressure of 20 mN/m, then equilibrated for 20 – 30 minutes. UV irradiation of the compressed films was performed with a pair of pen lamps (Oriol). UV exposure was controlled by setting the lamp height above the air-water interface and choosing specific exposure times as described elsewhere

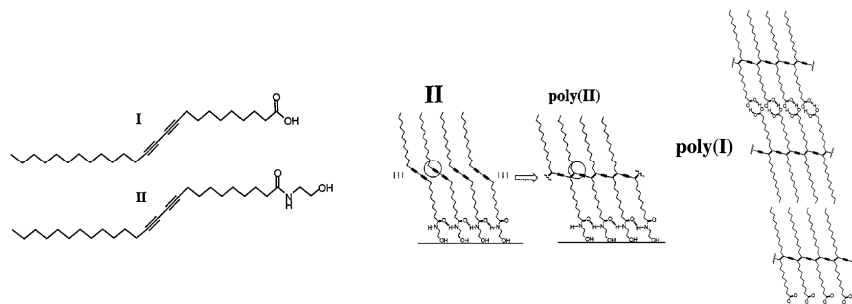


Figure 1. Left: PCDA (**I**) and PCEA (**II**) molecules. Middle: schematic of molecular orientation of **II** and its subsequent conversion to poly(**II**) upon UV irradiation. A hydrogen bonded network at the headgroup position in the monolayer is drawn. Right: poly(**I**) in its trilayer form. Hydrogen-bonded carboxylate dimers bind the top two layers to each other, and the lowest layer is bonded to the substrate through hydrogen bonds. Van der Waals' interactions bond the lowest and middle layers.

(22). A few minutes after UV exposure, the water was slowly drained off by aspiration. The films were laid down on mica (freshly cleaved) or silicon (piranha-cleaned) substrates that were pre-submerged horizontally in the aqueous subphase before monolayer spreading. The substrate was then removed and dried in clean room air. This horizontal transfer method proved to be the most effective for producing high quality films, as polymerization creates a degree of rigidity in the film on the water surface. This rigidity renders vertical transfer methods unreliable as the films would not uniformly compress during vertical transfer.

### Instrumentation

A Nanoscope IIIA AFM (Digital Instruments) operating in contact mode was used to obtain topographic and friction force images. The same type of AFM was used to obtain IC AFM measurements. AFM data were acquired under laboratory ambient conditions. Silicon nitride cantilevers (Digital Instruments) with a nominal normal force constant of 0.06 N/m were used for all contact-mode measurements. For IC-AFM images, Si cantilevers were used. A novel home-built NSOM (23) was used to simultaneously observe sample fluorescence with sub-wavelength resolution as well as normal forces and shear forces. The tips used were Al-coated etched optical fibers.

## Results and Discussion

### Film Structure

Pressure-area isotherms indicate the amphiphiles of **I** and **II** on pure water both had identical take-off areas of  $25 \text{ \AA}^2/\text{molecule}$ , corresponding to the molecular cross-section of the hydrocarbon-diacetylene structure. The film of **I** collapses at low pressure ( $\sim 12 \text{ mN/m}$ ), but upon over-compression reaches a stable solid phase with a limiting molecular area of  $\sim 8 \text{ \AA}^2/\text{molecule}$ . This over-compressed state corresponds to a stable trilayer structure. The film of **II** was stable as a monolayer with a collapse pressure of ca.  $35 \text{ mN/m}$  and an extrapolated molecular area at zero pressure of  $25 \text{ \AA}^2/\text{molecule}$ . After equilibration, films were polymerized to the blue-phase by exposure to incidence powers of  $40 \text{ \mu W/cm}^2$  for **I** and  $23 \text{ \mu W/cm}^2$  for **II** over a period of 30 sec. Red-phase films were produced by exposing the trilayer of **I** to  $500 \text{ \mu W/cm}^2$  and the monolayer of **II** to  $40 \text{ \mu W/cm}^2$  for 5 min.

AFM images of the blue- and red-phase forms of poly(**I**) and poly(**II**) on mica or silicon substrates confirm that the coverage for all films was nearly uniform for the entire substrate. Over 95% of the transferred film was flat to within  $\pm 0.5 \text{ nm}$ , with up to  $100 \text{ \mu m}$  crystalline domains observed. AFM measurements confirmed that films of **I** and **II** formed trilayers and monolayers respectively. There were distinct height differences between the blue- and red-phase films of both **I** and **II**. The heights of the blue- and red-phase trilayers of poly(**I**) were measured at  $7.4 \pm 0.8$  and  $9.0 \pm 0.9 \text{ nm}$ , respectively. The blue- and red-phase poly(**II**) monolayer films had similarly proportional height differences of  $2.7 \pm 0.3$  and  $3.1 \pm 0.3 \text{ nm}$ , respectively. The films possess highly aligned striations corresponding to small height variations of  $\sim 2 \text{ \AA}$  discussed further below, and similar to previous reports (9). These striations appear to be small variations in density or side chain tilt angle and are aligned with the polymer backbone direction, as confirmed with polarized fluorescence microscopy.

These results provide insight into the stabilization of diacetylene films. The headgroup interactions and alkyldiyne chain stacking should dominate the film structure of the monomeric diacetylene Langmuir films. The ability of the amide headgroup of **II** to form lateral intermolecular hydrogen bonded structures (Fig. 1, center), similar to  $\beta$ -sheets in proteins, may explain the stability of this monolayer film on pure water. In contrast, **I** films on pure water are unstable as monolayers but stack favorably into trilayers. Carboxylic acid dimer formation aids in stabilizing this structure. Indeed, stable bilayer islands are commonly observed on top of the **I** trilayer. Thus, by altering the head group, we can control whether the resulting film will be structured as a monolayer or a trilayer. Further details of the film preparation and structure are published elsewhere (22).

## Mechanochromism

The blue-to-red transition can be activated at the nanometer scale using NSOM or AFM tips on both the trilayer poly(I) and monolayer poly(II) (7,24). Fig. 2 shows simultaneous NSOM topography and fluorescence images on a blue poly(I) film. In the first scan (left pair), no fluorescence is seen over the flat PCDA region. In the subsequent scan (right pair), topographic changes are created, and localized fluorescence emission is produced. A fluorescence spectrum obtained over this region reveals the spectral fingerprint of red PCDA. These observations were reproducible. In general, when this transition is observed, the fluorescent regions grow in size with each image acquired.

The blue-to-red transition has also been produced using AFM tips with both trilayer poly(I) and monolayer poly(II) blue films (Fig. 3). With AFM, local topographic changes, discussed below, are observed *in-situ*. These changes indicate the transition is taking place. By creating a large ( $>1 \mu\text{m}$ ) red region, *ex-situ* fluorescence microscopy is used to confirm that a red region has been created by the AFM tip. With both AFM and NSOM, normal forces alone are not sufficient to cause the transition. Shear forces must also be applied, *i.e.* during the scanning process, to produce the blue-to-red transition. In all cases, the observed transitions are irreversible up to at least several months.

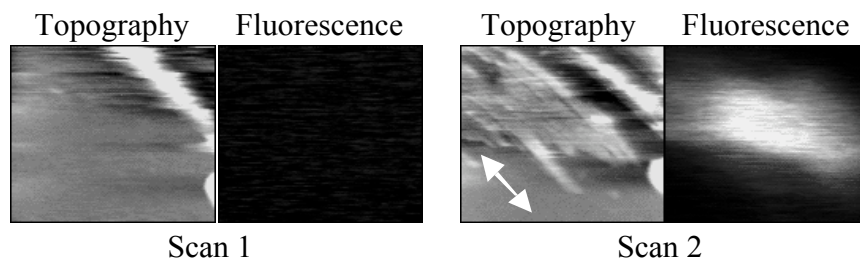
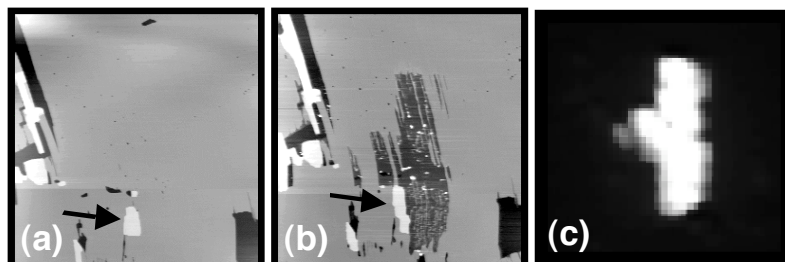


Figure 2. NSOM shear force topography and simultaneous fluorescence images ( $2.4 \times 2.4 \mu\text{m}^2$ ) showing tip-induced mechanochromism.



*Figure 3. 10 $\times$ 10  $\mu\text{m}^2$  topographic AFM images showing tip-induced patterning of red PCDA domains. (a) Initial image of a blue film. (b) Final image with a patterned red region. The backbones are oriented in roughly the vertical direction. The patterning was formed by multiple, high-load scans within the patterned region. The black arrow indicates a bilayer island that has grown in size after patterning. (c) Far-field fluorescence image of the same region. Characteristic red PCDA fluorescence is localized within the patterned region.*

The transformed regions consistently exhibit higher friction, increased roughness, and a surprising height reduction of typically 40-50% of the original film height. High resolution images of the transformed regions, however, consistently reveal backbone-related striations. This indicates a substantial degree of preservation of the conjugated backbone despite the dramatic height reduction. No such structural change for other types of PDA have been previously reported. While this height reduction could be explained by a removal of one or more layers in the trilayer poly(I) film, this cannot explain the comparable height reduction for the monolayer. One possibility is that some molecules are removed during the transformation process, and the remaining molecules substantially increase the tilt angle of the hydrocarbon side chains. The all-*trans* nature of the side chains may also be strongly disturbed, but the backbone structure remains. This increased tilt angle and conformational changes allow stress within the backbone and side chains to be relieved as discussed below. This picture is consistent with the observation via AFM that the backbones remain in tact, and the film is greatly compressed. It is also consistent with the observation that friction force between the tip and PDA sample is higher over the transformed region, since highly tilted and defective side chains would expose more methylene groups to the tip, as opposed to the terminal methyl groups which have a lower surface energy.

The blue phase therefore appears to be a metastable phase. On the Langmuir trough, the high registry of the diacetylene packing permits rapid topochemical polymerization of the diyne monomers to the ene-yne conjugation upon UV illumination resulting in the blue-phase polydiacetylene. Little change in the

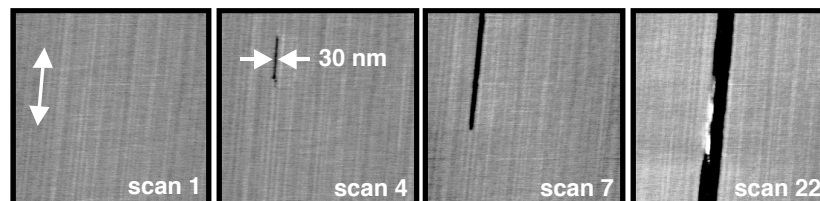


Figure 4. Series of  $1 \times 1 \mu\text{m}^2$  topographic AFM images of blue PCDA showing the progressive growth of the tip-induced red domains. In the first scan, striations indicative of the polymer backbone direction are observed. By the fourth scan, a topographically distinct (i.e. lower) region, only 30 nm wide, appears. This region continues to grow in subsequent scans.

amphiphile packing, and thus little reorientation of the alkyl side chains occurs. However, the hybridization change from  $sp$  to  $sp^2$  for the terminal alkyne carbons creates a stress on the polymer as a result of the  $180^\circ$  to  $120^\circ$  bond angle conversion (see Fig. 1). With initial UV illumination to create the blue form, significant molecular stress is built into the film. At higher degrees of polymerization, or with the application of mechanical stress or heat, the film's original structure breaks down as the alkyl chains of the blue-phase polymer reorganize to accommodate the bond angle conversion. In the case of UV polymerization or heating, this yields a closer packing (film contraction) and reorientation (vertical height increase) of the alkyl chains. In the case of mechanochromism, this leads to a totally different collapsed film structure.

These reorganizations, although thermodynamically more stable, produce a loss of  $\pi$ -conjugation and results in the red form of the polydiacetylene. These results are consistent with recent NMR investigations by Lee *et al.* (12) which show that the blue-to-red thermochromic transition in other PDA bulk samples involves a release of mechanical strain on the backbone and reorganization of the side groups. Furthermore, FTIR data of Lio *et al.* (9) and  $^{13}\text{C}$  NMR data of Tanaka *et al.* (25) suggest that some of the tilted side chains rotate toward the surface normal in the red phase for thermochromic films. Theoretical calculations indicate that a rotation of only a few degrees about this bond dramatically changes the  $\pi$ -orbital overlap (26), causing a significant blue-shift of the absorption spectrum. Recent molecular modeling studies (24) of PDA oligomers also show that a loss of backbone planarity leads to shifts in absorption spectra corresponding to the blue-to-red transition.

## Friction Anisotropy

AFM measurements demonstrate that the films possess strong friction anisotropy (21). For example, measurements on the red poly(II) monolayer (Fig. 5(a) and 5(b)) reveal a domain structure. The friction force varies substantially from one domain to the next, and is nearly uniform within each domain. The topographic image reveals an essentially flat film. As mentioned above, topographic images within a single domain reveal parallel striations of varying width and uniform direction (Fig. 4). These striations are associated with the direction of the underlying polymer backbone, and allow us to determine the relative angle between the sliding direction and the backbone direction.

By measuring the friction force at the same load for different orientations, we find that friction is lowest when sliding parallel to the backbones, and 2.9 times larger when sliding perpendicular (Fig. 5(c)). This dramatic effect may be due to anisotropic film stiffness caused by anisotropic packing and/or ordering of the alkyl side chains, as well as the anisotropic stiffness of the polymer backbone structure itself. Along the backbone direction, the conjugated polymer bonds provide a rigid link between alkyl chains (Fig. 1). However, the spacing between alkyl chains linked to *neighboring* backbones is determined by weaker interchain van der Waals' forces and head group-substrate interactions. In other words, the lack of covalent bonding between neighboring polymer chains allows some freedom in their spacing, consistent with previous studies of a similar PDA film (9). Variations in film density would also explain the typical film height contrast of  $\sim 2\text{\AA}$  due to the striations observed in Fig. 4 (27).

A simple model for a scalar in-plane anisotropic tip-sample interaction force  $F_{in-plane}$  is an isotropic dissipative force  $F_1$ , plus an anisotropic term that varies as  $\sin(\varphi)$  with maximum value  $F_2$ :

$$F_{in-plane} = F_1 + F_2 |\sin(\varphi)| \quad (1)$$

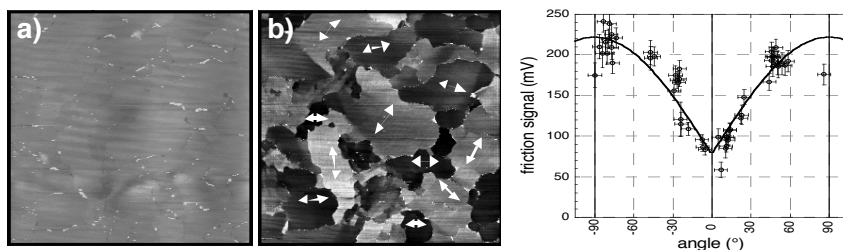


Figure 5. (a)  $50 \times 50 \mu\text{m}^2$  AFM topography image of a red poly(I) monolayer. (b) simultaneous friction image. The friction image reveals the different domains. White arrows indicate the domain orientation. (c) Friction force (raw signal units) vs. angle.  $0^\circ$  indicates sliding parallel to the backbone direction. The standard deviation is used for the friction error bars. The solid line represents the fit of Eq. (1) to the data.

where  $\varphi$  represents the domain orientation. The anisotropic term is consistent with the notion that the frictional work done is equal to the vector dot product of the distance traveled and a force that only acts perpendicular to the backbones. The absolute value is used to ensure that this contribution is positive. Eq. (1) provides a consistent fit to the data as shown in Fig. 5(c), giving  $F_1 = 77$  mV and  $F_2 = 144$  mV (uncalibrated raw signal units). Thus, according to the fit, the total friction anisotropy is  $F_{max} = \frac{F_1 + F_2}{F_1} = 2.9$ .

The anisotropic contribution  $F_2$  may have several sources. Lower stiffness along the perpendicular direction may lead to larger molecular deformation when sliding in that direction, and thus a larger contact area, more gauche defect creation, and more bending of the hydrocarbon chains. These would all contribute to larger friction forces (28).

### Imaging In-Plane Anisotropy with Intermittent Contact AFM

In IC AFM, the AFM cantilever is driven at or near its resonance frequency so that the tip oscillates with respect to the substrate. The tip makes contact with the sample for a small portion of its cycle, and the reduced amplitude that results is used as a feedback signal to map out the topography of the sample. The corresponding phase shift between the drive and response is monitored simultaneously, and is generally considered to be a map of dissipation during compression of the sample along the sample normal.

Fig. 6(a) shows an IC AFM topographic image of a PCEA monolayer film with large domains (29). Islands of extra PCEA layers are also visible. As with contact-mode AFM, each domain can be identified in the phase image by the orientation of the striations along which the PDA backbones lie (9,22). The typical phase  $\varphi$  in Fig. 6(b) is approximately  $116^\circ$  (30). Given that the properties of PDA films *normal* to the substrate are highly uniform between domains, it is surprising that the phase  $\varphi$  differs from domain to domain by up to  $2^\circ$  in Fig. 6(b). The maximum phase  $\varphi_{max}$  occurs when the long axis of the cantilever is parallel to the striations ( $\varphi = 0^\circ$ ).

Phase shifts in IC-AFM indicate energy loss (31). When the tip's motion is sinusoidal, the power dissipated due to the tip-sample interaction is (31,32):

$$\bar{P}_{tip} = \frac{1}{2} \frac{kA^2\varphi_0}{Q} \frac{\varphi A_0}{A} \sin(\varphi) \quad (2)$$

where  $\varphi$  is the phase of the oscillation relative to the drive,  $k$  is the spring constant of the cantilever,  $\varphi_0$  is the cantilever's resonance frequency,  $Q$  is the quality factor of the cantilever,  $A_0$  is the free oscillation amplitude of the lever, and  $A$  is the reduced amplitude during measurement. We have shown that, consistent with many IC-AFM measurements, the tip motion is very nearly sinusoidal in our experiments (29).

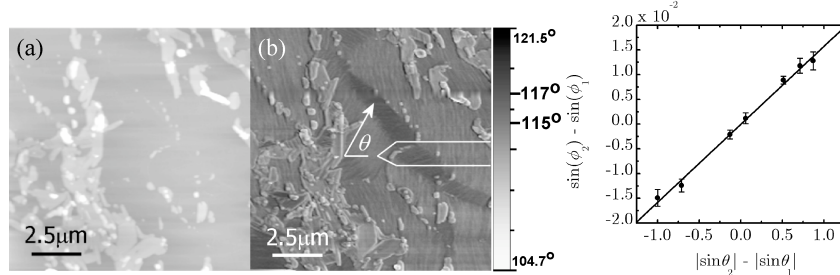


Figure 6. Topographic (a) and phase (b) images of a PDA monolayer thin film on mica.  $\theta$  is the angle between the local PDA backbone striations and the long axis of the cantilever. The orientation of the cantilever is sketched at the right.

(c) The difference in the sines of the phase angles  $\theta$  proportional to the difference in energy loss between domains, versus the difference in the absolute values of the sines of the angles  $\theta$  proportional to the difference in the in-plane tip-sample dissipative forces.

From Fig. 6(b) and Eq. (2), we find that the power dissipated is smallest (*i.e.* phase shift largest) when the striations are parallel to the long axis of the cantilever. In fact, the cantilever loses an extra amount of energy  $\Delta E \approx 2.4$  eV per cycle in domains where the striations are perpendicular, rather than parallel to the long axis of the cantilever. The effect observed in Fig. 6(b) can now be explained by considering the fact that the cantilever is tilted along its long axis ( $11^\circ$  in our case). Therefore, there will be a small but significant component of tip motion parallel to the sample during each oscillation cycle. The direction of larger dissipation corresponds, as we would expect, with the direction of high friction for this component of in-plane sliding. The amount of extra energy dissipated is roughly 10% of the total energy dissipated through the tip-sample interaction. That this level of energy loss should occur due to in-plane forces is reasonable, given that the tip moves in the plane of the sample a distance that is  $\sim 20\%$  of the total tip displacement.

Fig. 6(c) is a plot of  $\sin(\theta_2) - \sin(\theta_1)$  vs.  $|\sin \theta_2| - |\sin \theta_1|$  for the data in Fig. 6(b) (29). Remarkably, we find that  $\sin(\theta_2) - \sin(\theta_1)$  is proportional to  $|\sin \theta_2| - |\sin \theta_1|$ , with proportionality constant  $\beta = (1.58 \pm 0.05) \times 10^{02}$ . This linear proportionality is discussed in detail in reference (29). If Eq. (2) describes the power dissipation, the observed proportionality is expected. From Eq. (2), the difference in  $F_{in-plane}$  between two domains 1 and 2 is simply proportional to  $|\sin(\theta_2)| - |\sin(\theta_1)|$ . The difference in power dissipated between two domains is proportional to  $\sin(\theta_2) - \sin(\theta_1)$ , if we assume that Eq. (1) correctly describes the in-plane dissipation. We therefore conclude that the

anisotropic forces in our experiment arise from friction, or in addition, inelastic shear deformation.

We have constructed a model which, unlike previous models of IC-AFM, takes the tilt of the cantilever into account. The model assumes Hertzian tip-sample contact, with both in-plane and out-of-plane dissipative components (29). The key result is that components of motion both normal and parallel to the sample occur, and therefore in-plane dissipative processes can cause phase shifts. Using parameters appropriate for our system, we solve for the steady state motion of the tip. The model indicates a maximum tip-sample in-plane tip motion of  $\Delta x = 49.9 \pm 0.1$  pm parallel to the sample. The distance  $\Delta x$  is extremely small, and it is difficult to make firm distinctions between friction and shear deformation at such a small scale, as discussed below. The important result is that  $\Delta x$  is virtually independent of the in-plane damping. Furthermore, the model produces a nearly sinusoidal tip motion, indicating that Eq. (2) remains valid for the tilted-cantilever geometry.

In principle, modeling can be used to quantitatively associate the measured phase shifts with the dissipative in-plane properties of the material being imaged. These properties are friction (as quantified by the interfacial shear strength  $\tau$  between the tip and sample) (28) and dissipative shear deformation (due to viscoelasticity of the sample, as quantified by the loss tangent of the material,  $\tan \delta$ ) (33). Both of these mechanisms contribute to the observed dissipation and so we cannot explicitly separate them in our data. However, we can use our data to determine the upper limits of  $\tau$  and  $\tan \delta$  by finding the values that result when attributing all the dissipation to each mechanism respectively. The current difficulty with this approach is that the phase shifts predicted by our Hertzian model have the opposite sign to the phase shifts we observe. The reason for this discrepancy is that we have ignored adhesion in our model. Preliminary results from modeling that includes adhesion show that the phase shift changes sign and becomes consistent with our data. A description of this adhesive model is in progress (34).

## Conclusions

We have produced high-quality ultrathin PDA films using a horizontal Langmuir deposition technique. The number of stable layers in the film is controlled by altering the head group functionality. The films exhibit strong friction anisotropy that is correlated with the direction of the polymer backbone structure. Shear forces applied by AFM or NSOM tips locally induce the blue-to-red chromatic transition in the PDA films.

Monolayer films of PCEA exhibit strong threefold friction anisotropy. Friction is highest when scanning perpendicular to the polymer backbone direction. We propose that this effect results from anisotropic film deformation modes.

The highly anisotropic nature of PDA films allows us to show that in-plane properties of materials can be observed using IC-AFM. This is due to the tilt of the AFM cantilever which produces a small but significant in-plane component to the tip's motion. In the case of PDA monolayers, in-plane friction and shear deformation anisotropy leads to contrast in the IC-AFM phase image. The results can be explained using a simple model that incorporates Hertzian contact mechanics with in-plane dissipation, and may be generalized to the study of other anisotropic materials.

### Acknowledgement

We acknowledge funding from the NSF CAREER program, grant #DMR0094063 (MAE) and grant #CMS0134571 (RWC), the Research Corporation (MAE), and the NSF MRSEC program, grant #DMR0079983, and the University of Wisconsin-Madison. Some images in this paper were prepared using WSxM freeware from Nanotech Electronica. Sandia is a multiprogram laboratory operated by Sandia Corporation, a Lockheed Martin Company, for the United States Department of Energy under Contract DE-AC04-94AL85000.

### References

- (1) Ulman, A. *Introduction to Ultrathin Organic Films from Langmuir-Blodgett to Self-Assembly*; Academic Press: New York, 1991.
- (2) Schwartz, D. K. *Surf. Sci. Rep.* **1997**, *27*, 245.
- (3) Bloor, D.; Chance, R. R. *Polydiacetylenes: Synthesis, Structure, and Electronic Properties*; Martinus Nijhoff: Dordrecht, 1985.
- (4) Day, D.; Hub, H. H.; Ringsdorf, H. *Isr. J. Chem.* **1979**, *18*, 325.
- (5) Tieke, B.; Lieser, G.; Wegner, G. *J. Polym. Sci., A, Polym. Chem.* **1979**, *17*, 1631.
- (6) Olmsted, J.; Strand, M. *J. Phys. Chem.* **1983**, *87*, 4790.
- (7) Carpick, R. W.; Sasaki, D. Y.; Burns, A. R. *Langmuir* **2000**, *16*, 1270.
- (8) Wenzel, M.; Atkinson, G. H. *J. Am. Chem. Soc.* **1989**, *111*, 6123.
- (9) Lio, A.; Reichert, A.; Ahn, D. J.; Nagy, J. O.; Salmeron, M.; Charych, D. H. *Langmuir* **1997**, *13*, 6524.
- (10) Chance, R. R.; Baughman, R. H.; Muller, H.; Eckhardt, C. J. *J. Chem. Phys.* **1977**, *67*, 3616.
- (11) Carpick, R. W.; Mayer, T. M.; Sasaki, D. Y.; Burns, A. R. *Langmuir* **2000**, *16*, 4639.
- (12) Lee, D. C.; Sahoo, S. K.; Cholli, A. L.; Sandman, D. J. *Macromolecules* **2002**, *35*, 4347.
- (13) Muller, H.; Eckhardt, C. J. *Mol. Cryst. Liq. Cryst.* **1978**, *45*, 313.
- (14) Nallicheri, R. A.; Rubner, M. F. *Macromolecules* **1991**, *24*, 517.

- (15) Tomioka, Y.; Tanaka, N.; Imazeki, S. *J. Chem. Phys.* **1989**, *91*, 5694.
- (16) Cheng, Q.; Stevens, R. C. *Langmuir* **1998**, *14*, 1974.
- (17) Jonas, U.; Shah, K.; Norvez, S.; Charych, D. H. *J. Am. Chem. Soc.* **1999**, *121*, 4580.
- (18) Charych, D. H.; Nagy, J. O.; Spevak, W.; Bednarski, M. D. *Science* **1993**, *261*, 585.
- (19) Reichert, A.; Nagy, J. O.; Spevak, W.; Charych, D. *J. Am. Chem. Soc.* **1995**, *117*, 829.
- (20) Charych, D.; Cheng, Q.; Reichert, A.; Kuziemko, G.; Stroh, M.; Nagy, J. O.; Spevak, W.; Stevens, R. C. *Chemistry and Biology* **1996**, *3*, 113.
- (21) Carpick, R. W.; Sasaki, D. Y.; Burns, A. R. *Trib. Lett.* **1999**, *7*, 79.
- (22) Sasaki, D. Y.; Carpick, R. W.; Burns, A. R. *J. Colloid Interface Sci.* **2000**.
- (23) Burns, A. R.; Houston, J. E.; Carpick, R. W.; Michalske, T. A. *Langmuir* **1999**, *15*, 2922.
- (24) Burns, A. R.; Carpick, R. W.; Sasaki, D. Y.; Shelnutt, J. A.; Haddad, R. *Trib. Lett.* **2001**, *10*, 89.
- (25) Tanaka, H.; Gomez, M. A.; Tonelli, A. E.; Thakur, M. *Macromolecules* **1989**, *22*, 1208.
- (26) Orchard, B. J.; Tripathy, S. K. *Macromolecules* **1986**, *19*, 1844.
- (27) Fenter, P.; Eisenberger, P.; Liang, K. S. *Phys. Rev. Lett.* **1993**, *70*, 2447.
- (28) Carpick, R. W.; Salmeron, M. *Chem. Rev.* **1997**, *97*, 1163.
- (29) Marcus, M. S.; Carpick, R. W.; Sasaki, D. Y.; Eriksson, M. A. *Phys. Rev. Lett.* **2002**, *88*, 226103.
- (30) The reported phase shifts are true phase shifts with respect to the drive signal. The phase shifts reported by the instrument are not properly scaled and are shifted by 90°.
- (31) Cleveland, J. P.; Anczykowski, B.; Schmid, A. E.; Elings, V. B. *Appl. Phys. Lett.* **1998**, *72*, 2613.
- (32) Tamayo, J.; Garcia, R. *Appl. Phys. Lett.* **1997**, *71*, 2394.
- (33) Lakes, R. S. *Viscoelastic solids*; CRC Press: Boca Raton, 1999.
- (34) D'Amato, M. J.; Marcus, M. S.; Eriksson, M. A.; Carpick, R. W.; in preparation.